PET and MRI of Metastatic Peritoneal and Pulmonary Colorectal Cancer in Mice with Human Epidermal Growth Factor Receptor 1–Targeted ^{89}Zr-Labeled Panitumumab

Tapan K. Nayak, Kayhan Garmestani, Diane E. Milenic, and Martin W. Brechbiel

Radioimmune and Inorganic Chemistry Section, Radiation Oncology Branch, National Cancer Institute, National Institutes of Health, Bethesda, Maryland

Human epidermal growth factor receptor 1 (*HER1*) plays an important role in the pathogenesis of colorectal cancer. Panitumumab is an anti-*HER1* monoclonal antibody approved for use in colorectal cancer. However, few data exist regarding *HER1* status in the corresponding distant metastases, and little corresponding information is available regarding the localization of panitumumab at primary and metastatic lesions. The utility of PET and MRI using ^{89}Zr-panitumumab to assess the status of *HER1* in distant metastases with different metastasis models is presented in this study. **Methods:** In vivo biodistribution and PET studies were performed in *HER1*-expressing LS-174T and *HER1*-negative A375 tumor xenografts. Additionally, studies were performed in different models of intraperitoneal and pulmonary metastases. MRI studies were performed for metastatic models to characterize the targeting potential of ^{89}Zr-panitumumab at different lesion sites. **Results:** *HER1*-mediated targeting was achieved in all *HER1*-expressing models. The LS-174T tumor area under the curve (AUC) was 3.7-fold greater than the AUC for A375. The LS-174T tumor AUC of 204.13 ± 9.67 was significantly greater ($P < 0.001$) than the LS-174T tumor AUC of 36.45 ± 1.39 obtained from mice coinjected with 0.1 mg of panitumumab for blocking the target. Differences were observed in 2 intraperitoneal models; tumor uptake in mice with a 3-d tumor burden was more than 2-fold greater than the mice with a 7-d tumor burden. PET and MRI studies revealed *HER1*-mediated tumor targeting in all metastatic models. However, significant differences were observed between different LS-174T tumor models. Peak tumor uptake of approximately 40 percentage injected dose per gram (%ID/g) was observed at 3–4 d after injection for the subcutaneous tumor model, in contrast to approximately 75 %ID/g at 2 d after injection for the thoracic tumors and approximately 95 %ID/g at 1–2 d after injection for the intraperitoneal tumors. **Conclusion:** The potential utility of ^{89}Zr-panitumumab in assessing *HER1* status in distant metastases and understanding the variations in antibody uptake at different lesion sites is demonstrated in this study. ^{89}Zr-panitumumab can play a vital role in patient stratification and immunotherapy and therefore warrants further investigation for clinical translation.

Key Words: immunoPET; PET; MRI; *HER1*; metastatic colorectal cancer; panitumumab; ^{89}Zr

J Nucl Med 2012; 53:113–120
DOI: 10.2967/jnumed.111.094169

Colorectal cancer (CRC) is 1 of the 3 most frequent malignancies in humans and is the third and fourth leading type of cancer in women and men, respectively (*1*). More than 30% of colorectal cancer patients develop peritoneal metastases carcinomatosis, with a medial survival of less than 6–8 mo (*2*). Pulmonary metastasis is known to be the most common extraabdominal site of metastases from CRC, and surgical intervention remains the proposed choice of treatment for metastatic sites (*3*).

Panitumumab (Vectibix; Amgen) is a fully human IgG_2 monoclonal antibody (mAb) that targets the extracellular domain of the human epidermal growth factor receptor 1 (*HER1*). *HER1* is a transmembrane cell surface glycoprotein belonging to the subfamily of type I tyrosine kinase receptors. Approximately 60%–70% human colorectal cancers express *HER1* (*4,5*). The expression of *HER1* is often associated with an aggressive form of disease and poor prognosis (*6,7*).

A critical factor in screening patients for targeted therapy is evaluating the presence and amount of the specific target in the tumor and its relevance to the disease state. Initial clinical experience with both cetuximab and panitumumab therapy revealed that *HER1* levels detected by immunohistochemistry did not correlate with response to anti-*HER1* immunotherapy (*8,9*). Besides factors such as v-kis-ras2 Kirsten rat sarcoma viral oncogene (KRAS) mutations, another possible reason might be possible differences in the *HER1* status between the primary and metastatic tumor sites and the accessibility of the antibody to different lesion sites. Unfortunately, there are limited data describing the *HER1* status in the primary colorectal tumor and the corresponding distant metastases. Imaging techniques such as PET and MRI provide insights into the tumor biology and are often clinically useful for establishing patient prognosis and deciding the best therapeutic option. Radiolabeled antibod-

Received Jun. 10, 2011; revision accepted Sep. 6, 2011.
For correspondence or reprints contact: Tapan K. Nayak, 10 Center Dr., MSC 1002, Room B3B69, NCI-Bethesda, Bethesda, MD 20892.
E-mail: tapann@gmail.com

ies have been used to confirm target expression and binding sites and as imaging agents to obtain better insight into the in vivo behavior and efficacy of the mAbs in individual patients (*10–12*). Preclinical PET studies of panitumumab labeled with ^{64}Cu (half-life, 12.7 h) and ^{86}Y (half-life, 14.7 h) have been reported (*13–15*). Although the preclinical studies demonstrated adequate tumor targeting, the half-lives of ^{64}Cu and ^{86}Y may limit quantitative imaging beyond 3 d after injection. Therefore, ^{89}Zr (with a longer half-life of 78.4 h) may be a better choice for clinical applications. Recently, ^{89}Zr-trastuzumab was evaluated for imaging *HER2* expression in *HER2*-positive metastatic breast cancer patients. PET images revealed a high spatial resolution and a good signal-to-noise ratio, resulting in better image quality than ^{111}In-trastuzumab SPECT scans (*16*). Excellent tumor uptake and visualization of metastatic liver, lung, bone, and even brain *HER2*-positive lesions were obtained 4–5 d after injection.

Considering the success of ^{89}Zr-trastuzumab in quantitative visualization of *HER2*-positive lesions in metastatic breast cancer, in this study we aimed to develop ^{89}Zr-panitumumab as a potential PET agent for potential use in risk stratification and quantitative noninvasive imaging of *HER1* and assessment of panitumumab uptake in primary tumor and distant metastases.

MATERIALS AND METHODS

Cell Lines and Tissue Culture

All cell lines were purchased from American Type Culture Collection (ATCC). *HER1*-expressing human colorectal adenocarcinoma LS-174T (ATCC no. CL-188), human epidermoid carcinoma A431 cells (ATCC no. CL-1555), and *HER-1*–negative human malignant melanoma A375 cells (ATCC no. CL-1619) were grown as a monolayer at 37°C, in a humidified atmosphere of 5% CO_2 and 95% air. LS-174T and A431 cells were cultured in Dulbecco minimal essential medium containing 10% FetaPLEX (Gemini Bio-Products), and 10 mM glutamine solution. A375 cells were cultured in Dulbecco minimal essential medium containing 10% FetaPLEX supplemented with 1 mM sodium pyruvate and insulin (10 μg/mL). Medium and supplements were obtained from Quality Biologicals, Invitrogen, or Lonza.

Production and Preparation of ^{89}Zr-Labeled Panitumumab

^{89}Zr was produced and purified at the National Institutes of Health, Bethesda (details provided in the supplemental information, available online only at http://jnm.snmjournals.org). The bifunctional chelator *p*-isothiocyanatobenzyl-desferrioxamine B (Df-Bz-NCS) (Macrocylics) was conjugated to panitumumab for radiolabeling with ^{89}Zr (details provided in supplemental information). The chelate-to-protein product ratio was determined by the isotope dilution method as previously described, using high-purity nonradioactive $ZrCl_4$ solution (*17,18*). For radiolabeling, 37−370 MBq of the ^{89}Zr-oxalate solution (pH ≤ 1) was neutralized to pH 7–7.5 by the slow addition of 2 M Na_2CO_3, followed by 0.5 M *N*-(2-hydroxyethyl)piperazine-*N*′-(2-ethanesulfonic acid) (HEPES) buffer. Alternatively, 5 M ammonium acetate was used instead of 0.5 M HEPES buffer to neutralize the solution after the slow addition of 2 M Na_2CO_3. A freshly prepared solution of gentisic acid (50 μL, 220 μg/μL) was then added to the solution to prevent radiolysis of the mAb, followed by 0.1 mg of panitumumab in 0.15 M ammonium acetate buffer. The reaction mixture was gently stirred and incubated at room temperature for 1 h. The reaction was quenched by the addition of ethylenediaminetetraacetic acid solution (4 μL, 0.1 M). The radiolabeled product was purified using a PD-10 desalting column (GE Healthcare). Size-exclusion high-performance liquid chromatography and cell-based immunoreactivity assays were performed to ascertain the purity and biologic integrity of the radioimmunoconjugate using previously described methods (*14,19,20*).

Animal Models

All animal studies were performed in accordance with the guidelines for the humane use of animals from the National Institutes of Health, and all procedures were reviewed and approved by the National Cancer Institute Animal Care and Use Committee. For subcutaneous tumor xenograft models, female athymic *nu/nu* mice (Charles River Laboratories) were injected subcutaneously with 2×10^6 *HER1*-expressing human colorectal adenocarcinoma LS-174T or 4×10^6 *HER1*-negative human melanoma A375 cells in 200 μL of corresponding medium containing 20% Matrigel (BD Biosciences). The aggressive metastatic disseminated peritoneal colorectal carcinoma model was developed by intraperitoneal injection of 1×10^8 *HER1*-expressing human colorectal carcinoma LS-174T in 1 mL of the medium, as previously described (*21*). For the pulmonary metastatic colorectal carcinoma model, 2×10^6 *HER1*-expressing human colorectal carcinoma LS-174T cells in 50 μL of corresponding medium were directly injected in the thoracic cavity by advancing the needle approximately 5 mm through the fourth intercostal space into the right lateral thorax.

Biodistribution Studies

The biodistribution studies for female athymic mice were performed as follows. Those mice bearing *HER1*-expressing human colorectal LS-174T ($n = 5$) and *HER1*-negative human melanoma A375 ($n = 5$) subcutaneous tumor xenografts were intravenously injected with 0.4–0.6 MBq (<5 μg) of ^{89}Zr-labeled panitumumab, those bearing disseminated peritoneal LS-174T carcinoma ($n = 5$) were administered 0.4–0.6 MBq (<5 μg) of ^{89}Zr-labeled panitumumab by intraperitoneal injection 3 d after the inoculation of LS-174T cells in the peritoneal cavity, and those bearing pulmonary metastatic LS-174T carcinoma ($n = 5$) were administered 0.4–0.6 MBq (<5 μg) of ^{89}Zr-labeled panitumumab by intravenous injection 5 d after the inoculation of LS-174T cells in the thoracic cavity. To demonstrate *HER1* specificity, excess mAb (0.1 mg) was coinjected with the radioimmunoconjugate into an additional set of mice ($n = 5$) bearing corresponding tumors. At the desired times, the animals were sacrificed by CO_2 inhalation. Tumor, blood, and selected organs were harvested and wet-weighed, and the radioactivity was measured in a Wizard 1480 γ-counter (PerkinElmer). The tissue percentage injected dose per gram (%ID/g) was calculated by comparison using standards representing 10% of the injected dose per animal. Noncompartmental pharmacokinetics were performed to determine area under the curve (AUC) using trapezoidal integration analysis (*22*).

PET

Small-animal PET studies were performed using the Siemens Focus 120 scanner at the National Institutes of Health. Whole-body imaging studies (single bed position; total acquisition time, 1 h per mouse) were performed on mice anesthetized with 1.5%–1.7%

isoflurane on a temperature-controlled bed, as previously described (*14*). Female athymic mice bearing subcutaneous and pulmonary tumors were injected intravenously with 1.7–1.9 MBq (<5 μg) of ^{89}Zr-labeled panitumumab, and for mice bearing intraperitoneal tumors, 1.7–1.9 MBq (<5 μg) of ^{89}Zr-labeled panitumumab were injected (intraperitoneally). The radioimmunoconjugate was injected in 2 sets of mice—one set comprised mice bearing intraperitoneal tumors with a 3-d tumor burden and another set comprised a 7-d tumor burden, representing relatively early-stage and late-stage disease, respectively. Additionally, non–tumor-bearing mice were injected (intravenously or intraperitoneally) with the equivalent radioimmunoconjugate as controls. To determine *HER1* specificity in mice bearing subcutaneous tumor xenografts, excess unmodified mAb (0.1 mg) was coinjected with the ^{89}Zr-labeled panitumumab. A 10-min transmission scan was obtained with a precalibrated ^{57}Co sealed source for attenuation correction for mice bearing pulmonary or intraperitoneal tumors. ^{89}Zr-filled cylinder phantoms were imaged during each imaging session for normalization and quantitative analysis. Further details regarding image acquisition, processing, and analysis are provided in the supplemental information.

MRI

After the PET session, MRI was performed on those mice bearing peritoneal and pulmonary LS-174T tumors using a 3-T MRI clinical scanner (Intera; Philips Medical System) with a dedicated 40-mm-inner-diameter solenoid coil (Philips). Mice were euthanized immediately after PET and sealed in plastic tubes. MRI was performed within 6 h of euthanasia. T2-weighted images were acquired with the following parameters: field of view, 8.0 × 8.0 × 2.0 cm; data matrix, 512 × 512; 40 slices; echo time/repetition time, 65/4,500; flip angle, 90°; slice thickness, 0.5 mm; in-plane resolution, 0.156 × 0.156 mm; and scan time, approximately 10–15 min.

Statistical Analysis

All numeric data were expressed as the mean of the values ± the SEM. Prism (version 5; GraphPad Software) was used for statistical analysis. A P value of less than 0.05 was considered statistically significant.

RESULTS

Radiochemistry and In Vitro Evaluations

Panitumumab was modified with the acyclic bifunctional chelator Df-Bz-NCS at a 5:1 molar excess of chelate to protein, yielding a final chelate-to-protein ratio of 1.7 ± 0.3 chelate molecules per protein molecule. The ^{89}Zr-labeled panitumumab conjugate was successfully prepared, with the radiochemical yields ranging from 80% to 95% and the highest specific activity in the range of 2.0–2.5 GBq/mg. Greater radiochemical yields were achieved when 0.5 M HEPES buffer was used instead of 5 M ammonium acetate buffer for neutralizing the pH to 7–7.5 (90%–95% vs. 80%–85%). The ^{89}Zr-labeled panitumumab conjugate demonstrated acceptable in vitro receptor specificity, as exhibited by a specific binding (%) of 72.39 ± 5.23 and nonspecific binding (%) of 5.03 ± 2.33 (n = 3) on fixed cells. The in vitro binding characteristics were comparable to previously reported ^{111}In- and ^{86}Y-labeled panitumumab (*14,19*).

In Vivo Evaluations: Biodistribution Studies

Subcutaneous Tumor Xenograft Model. In mice bearing LS-174T tumor subcutaneous xenografts, a 3.5-fold decrease in the blood-pool activity was observed over a 9-d period (11.47 ± 1.37 %ID/g at 1 d to 3.25 ± 0.34 %ID/g at 9 d) (Fig. 1A). Similarly, a 4.2-fold decrease in liver uptake was also observed (9.02 ± 0.29 %ID/g at 1 d to 2.18 ± 0.20 %ID/g at 9 d) (Fig. 1A). In contrast, tumor uptake of 27.92 ± 3.47 %ID/g at 1 d was similar to the tumor uptake of 25.65 ± 1.73 %ID/g observed at 9 d, with a peak tumor uptake of 42.89 ± 4.49 %ID/g at 3 d after injection, demonstrating retention of the radioimmunoconjugate in the tumor over the 9-d study period (Fig. 1A). The tumor-to-blood ratio increased 3.3-fold, 2.4 at 1 d to 7.9 at 9 d after injection. A significant increase in femur uptake was observed over 9 d (1.58 ± 0.17 %ID/g at 1 d to 6.94 ± 0.17 %ID/g at 9 d), indicating possible metabolism and localization of ^{89}Zr species into the bone. The ^{89}Zr-labeled panitumumab uptake in *HER1*-expressing LS-174T tumor subcutaneous xenografts was *HER1*-mediated, as demonstrated by the receptor-blocking experiments performed using a coinjection of 0.1 mg of panitumumab (Fig. 1B). The tumor uptake of 32.14 ± 1.41 %ID/g at 6 d was significantly greater than tumor uptake of 6.98 ± 0.52 %ID/g at 6 d in mice coinjected with 0.1 mg of panitumumab, thus demonstrating specificity of the radioimmunoconjugate (Fig. 1B). In contrast, no significant difference in tumor uptake was observed in *HER1*-negative mice bearing *HER1*-negative A375 tumor xenografts coinjected with 0.1 mg panitumumab (Fig. 1B).

Metastatic Intraperitoneal Colorectal Carcinoma Model. A significant decrease in blood-pool activity was observed over a 7-d period (12.85 ± 1.22 %ID/g at 1 d to 0.42 ± 0.06 %ID/g at 7 d) (Table 1). The tumor uptake decreased from 96.58 ± 8.97 %ID/g at 1 d to 17.71 ± 3.09 %ID/g at 7 d. Interestingly, a linear correlation (r^2 = 0.85) was observed between the tumor uptake expressed as %ID/g and tumor burden expressed as log (total tumor weight) (Fig. 2). The tumor-to-blood ratio increased more than 5-fold, from 7.5 at 1 d to 41.6 at 7 d after injection (Table 1). Similar to the subcutaneous LS-174T tumor xenograft model, a 2-fold increase in femur uptake was observed (3.00 ± 0.37 %ID/g at 1 d to 7.00 ± 1.32 %ID/g at 7 d), indicating possible metabolism and localization of ^{89}Zr species into the bone.

Metastatic Pulmonary Colorectal Carcinoma Model. Tumor uptake was similar throughout the observation period of 5 d, with the peak uptake of 78.05 ± 7.15 %ID/g at 2 d after injection (Table 2). The tumor-to-blood ratio increased 5.8-fold, from 3.0 at 1 d to 17.3 at 5 d after injection. The tumor uptake of 61.97 ± 6.02 %ID/g at 5 d was significantly greater than tumor uptake of 11.61 ± 1.26 %ID/g at 5 d in mice coinjected with 0.1 mg of panitumumab, demonstrating specificity of the radioimmunoconjugate.

In Vivo Evaluations: Imaging Studies

PET in Subcutaneous Tumor Xenograft Models. PET studies in female athymic mice bearing *HER1*-expressing

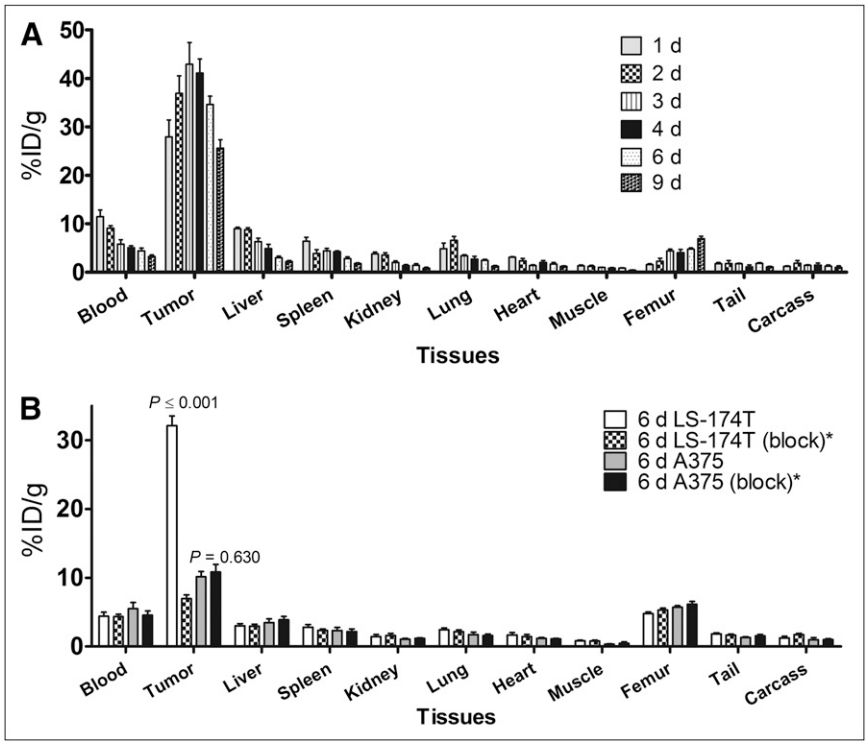

FIGURE 1. Biodistribution of ^{89}Zr-labeled panitumumab in selected organs of female athymic (NCr) *nu/nu* mice bearing *HER1*-positive subcutaneous LS-174T tumor xenografts (A) and receptor blocking in *HER1*-positive subcutaneous LS-174T tumor xenografts and *HER1*-negative subcutaneous A375 tumor xenografts (B). All values are expressed as %ID/g. Data represent mean value ± SEM from at least 4 determinations. *Receptor blocking studies were performed by coinjection of 0.1 mg of panitumumab with radiolabeled antibody.

LS-174T and *HER1*-negative A375 subcutaneous tumor xenografts were performed after intravenous injection of 1.7–1.9 MBq (<5 μg) of ^{89}Zr-labeled panitumumab. To determine *HER1* specificity, another set of tumor-bearing mice was coinjected with 0.1 mg of panitumumab to block the target. LS-174T tumor xenografts were clearly visible throughout the study period (1–6 d), with minimal background activity (Fig. 3A; Supplemental Fig. 1). In mice coinjected with 0.1 mg of panitumumab, tumors were poorly visualized (Fig. 3B; Supplemental Fig. 1), demonstrating *HER1* specificity. The PET images for all time points are provided in the supplemental information. Time–activity curves were generated to calculate the AUC as a measure of cumulative activity. The calculated AUC values from 0 to 6 d ($AUC_{[0\rightarrow 6\ d]}$) were expressed as %ID·d·g^{-1} (assuming 1 g = 1 cm^3). The *HER1*-expressing LS-174T tumor $AUC_{[0\rightarrow 6\ d]}$ of 204.13 ± 9.67 was 3.7-fold greater than the *HER1*-negative A375 tumor $AUC_{[0\rightarrow 6\ d]}$ of 54.45 ± 6.60 (Supplemental Fig. 2). The LS-174T tumor $AUC_{[0\rightarrow 6\ d]}$ of 204.13 ± 9.67 was significantly greater ($P < 0.001$) than the LS-174T tumor $AUC_{[0\rightarrow 6\ d]}$ of 36.45 ± 1.39 obtained from mice coinjected with 0.1 mg of panitumumab for blocking the target. However, for *HER1*-negative A375 tumors, there was no significant difference ($P = 0.166$) between AUC values obtained from mice injected with or without 0.1 mg of panitumumab (Supplemental Fig. 2). Liver and tumor uptake quantified by PET was closely related ($r^2 = 0.95$, $P = 0.97$, $n = 12$) to values determined by in vivo biodistribution studies.

PET and MRI in Metastatic Intraperitoneal Colorectal Carcinoma Model. PET was performed in non–tumor-bear-

TABLE 1
Biodistribution of ^{89}Zr-Labeled Panitumumab in Selected Organs of Female Athymic (NCr) *nu/nu* Mice Bearing Intraperitoneal Human LS-174T Tumors (3-Day Burden)

Tissue	1 d	2 d	3 d	5 d	7 d
Blood	12.85 ± 1.22	8.31 ± 1.63	3.63 ± 1.08	0.78 ± 0.11	0.42 ± 0.06
Tumor	96.58 ± 8.97	98.50 ± 15.65	53.48 ± 8.41	24.23 ± 3.25	17.71 ± 3.09
Liver	5.64 ± 0.91	6.13 ± 0.80	4.85 ± 0.39	3.90 ± 0.21	4.41 ± 0.37
Spleen	4.98 ± 0.92	7.03 ± 1.22	3.97 ± 0.47	4.85 ± 1.02	3.84 ± 0.56
Kidney	4.15 ± 0.28	4.49 ± 0.82	4.15 ± 0.64	3.56 ± 0.21	3.70 ± 0.36
Lung	6.07 ± 0.61	4.57 ± 0.65	2.47 ± 0.62	1.14 ± 0.40	1.02 ± 0.12
Heart	4.32 ± 0.53	2.78 ± 0.46	1.40 ± 0.31	0.54 ± 0.04	0.54 ± 0.06
Femur	3.00 ± 0.37	4.76 ± 0.68	5.50 ± 0.33	6.51 ± 0.72	7.00 ± 1.32
Tumor/blood	7.54 ± 0.19	12.28 ± 0.62	16.76 ± 1.97	31.96 ± 2.45	41.59 ± 3.87

Biodistribution data were obtained at 1, 2, 3, 5, and 7 d after intraperitoneal injection of ^{89}Zr-labeled panitumumab. All values are expressed as %ID/g (except ratios). Data represent mean value ± SEM from at least 5 determinations.

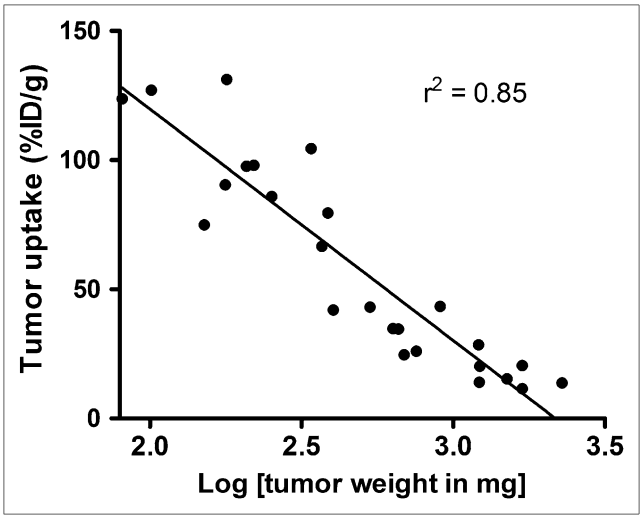

FIGURE 2. Correlation of tumor uptake expressed as %ID/g and tumor burden expressed as total tumor weight in female athymic (NCr) *nu/nu* mouse bearing intraperitoneal LS-174T tumors injected with ^{89}Zr-panitumumab.

ing mice and mice bearing intraperitoneal LS-174T tumors (3- and 7-d tumor burden representing early- and late-stage disease, respectively). All mice were injected intraperitoneally with 1.7–1.9 MBq (<5 μg) of ^{89}Zr-labeled panitumumab. After the completion of the PET study at 5 d, T2-weighed MRI was performed to localize tumors and correlate the localization of the radioactivity as observed by PET and therefore determine the tumor-targeting characteristics of the radioimmunoconjugate. In mice with a 3-d tumor burden, at 1 d, radioactivity was visualized along the peritoneal walls, liver lobes (expected localization of tumors), and heart and lung (blood pool) (Fig. 4A). Over a period of 5 d, the radioactivity was primarily localized around the peritoneal walls and liver lobes and cleared from the blood pool. The areas of radioactivity localization correlated with the tumor nodules found in the liver lobes and peritoneal walls as observed by MRI and postmortem dissection. MRI also revealed minor ascites along the peritoneal cavity (area with high contrast). The tumor nodules were removed postmortem, and radioactivity was measured to confirm the observation from PET and MRI. A similar pattern was observed in mice with a 7-d tumor burden; however, more aggressive growth and spread of the tumor was visualized over 1, 3, and 5 d after injection by a significant increase in the area of radioactivity localization (Fig. 4B; Supplemental Fig. 3). MRI revealed significant ascites around the tumors in the peritoneal cavity and the liver lobes, and significant accumulation of ascites was also observed along the diaphragm wall. The largest cancerous mass (over 1 cm^3) was observed along the peritoneal walls of mice with a 7-d tumor burden at day 5 of imaging. In non–tumor-bearing mice, most of the radioactivity was localized in the organs, such as heart and lung, representing blood-pool activity (Fig. 4C). No significant accumulation of radioactivity was observed in the peritoneal area. Similar to the biodistribution data, counts per cubic centimeter decreased with increasing tumor burden and growth. At 5 d, the counts per cubic centimeter in the tumor region with highest intensity from mice with a 3-d tumor burden were more than 2-fold greater than the corresponding counts in the group of mice with a 7-d tumor burden.

PET and MRI in Metastatic Pulmonary Colorectal Carcinoma Model. PET was performed in non–tumor-bearing mice and mice bearing pulmonary LS-174T tumors (5-d tumor burden). All mice were injected intravenously with 1.7–1.9 MBq (<5 μg) of ^{89}Zr-labeled panitumumab (Fig. 5; Supplemental Fig. 4). After completion of PET at 5 d, T2-weighed MRI was performed to localize tumors and correlate localization of the radioactivity as observed by PET and therefore determine the tumor-targeting characteristics of the radioimmunoconjugate. In tumor-bearing mice, 1 d after injection, most of the radioactivity accumulated in the thoracic region, with significant accumulation of radioactivity on the left side (seen as a bright spot from the dorsal view) (Fig. 5A). Over a period of 3 and 5 d, the blood-pool activity decreased significantly, whereas the ac-

TABLE 2
Biodistribution of ^{89}Zr-Labeled Panitumumab in Selected Organs of Female Athymic (NCr) *nu/nu* Mice Bearing Pulmonary Metastatic Human LS-174T Tumors

Tissue	1 d	2 d	3 d	5 d	5 d (block)*
Blood	19.77 ± 0.06	11.11 ± 0.73	6.32 ± 1.41	3.70 ± 0.42	14.11 ± 3.44
Tumor	59.95 ± 3.15	78.05 ± 7.15	60.12 ± 6.94	61.97 ± 6.02	11.61 ± 1.26
Liver	7.64 ± 0.53	6.13 ± 0.88	13.64 ± 6.73	8.67 ± 0.81	6.81 ± 0.72
Spleen	5.71 ± 0.20	4.63 ± 0.45	5.68 ± 0.45	5.91 ± 1.43	5.39 ± 1.28
Kidney	4.27 ± 0.32	3.46 ± 0.13	2.97 ± 0.60	3.00 ± 0.22	3.57 ± 0.41
Lung	13.86 ± 1.14	9.60 ± 1.36	7.69 ± 1.42	8.56 ± 2.31	5.07 ± 1.14
Heart	4.92 ± 0.31	3.56 ± 0.29	2.67 ± 0.55	1.64 ± 0.08	4.50 ± 0.53
Femur	3.60 ± 0.18	4.04 ± 0.14	5.07 ± 0.57	6.40 ± 0.96	3.51 ± 1.03
Tumor/blood	3.03 ± 0.15	7.09 ± 0.64	11.07 ± 1.79	17.26 ± 2.05	0.91 ± 0.17

*Receptor-blocking studies were performed by coinjecting 0.1 mg of panitumumab with radiolabeled antibody.

Biodistribution data were obtained at 1, 2, 3, and 5 d after intravenous injection of ^{89}Zr-labeled panitumumab. All values are expressed as %ID/g (except ratios). Data represent mean value ± SEM from at least 4 determinations.

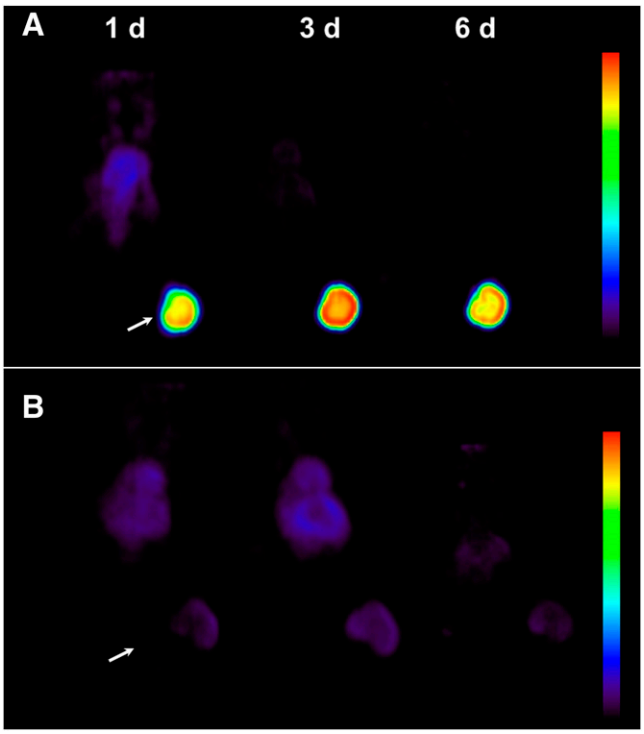

FIGURE 3. Representative reconstructed and processed maximum-intensity projections of female athymic (NCr) *nu/nu* mouse bearing subcutaneous LS-174T tumor xenograft intravenously injected via tail vein with 1.7–1.9 MBq of ^{89}Zr-labeled panitumumab (A) or 1.7–1.9 MBq of ^{89}Zr-labeled panitumumab coinjected with 0.1 mg of panitumumab for receptor blocking (B). Scale represents percentage of maximum and minimum threshold intensity. Tumors are indicated with arrows.

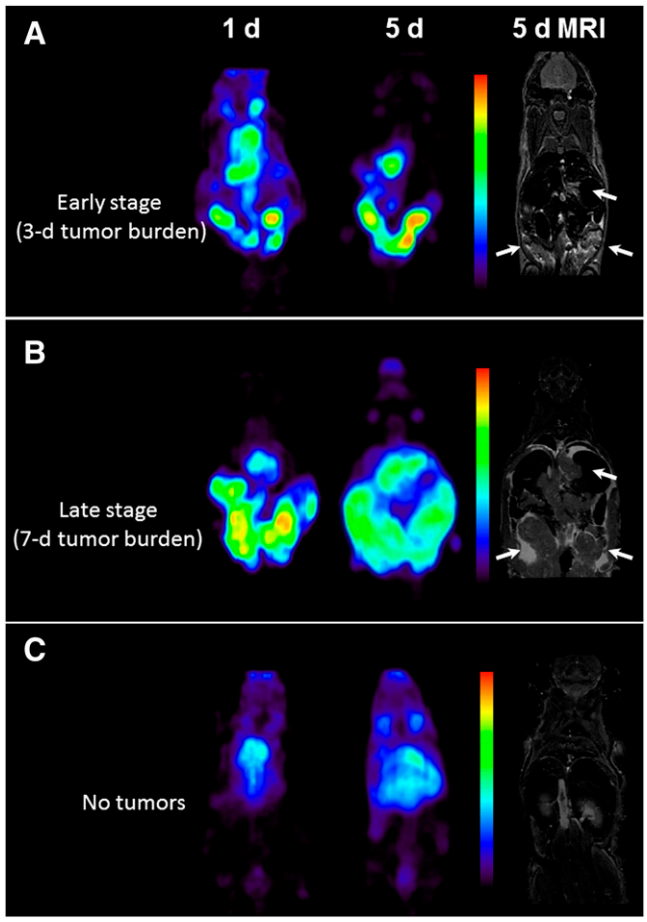

FIGURE 4. Representative reconstructed and processed maximum-intensity PET projections and corresponding T2-weighed coronal MRI slice of female athymic (NCr) *nu/nu* mouse bearing intraperitoneal LS-174T tumors (3-d burden) (A), mouse bearing intraperitoneal LS-174T tumors (7-d burden) (B), and non–tumor-bearing mouse (C). Scale represents percentage of maximum and minimum threshold intensity. Tumors are indicated with arrows.

tivity increased in the thoracic region (bright spots), indicating possible tumor locations (Fig. 5A; Supplemental Fig. 4). The accumulation of radioactivity in the thoracic region was significantly lower in non–tumor-bearing mice (Fig. 5B). MRI performed at 5 d after injection confirmed the tumor in the left corner of the thoracic cavity, where the radioactivity had accumulated. The tumor nodules were in the range of 70–150 cm^3. Additionally, significant effusion (high contrast) was observed above the diaphragm and thoracic region and pleural lining. However, a significant tumor mass was not detected in the upper thoracic region where 2 other bright spots from PET were located. On further observation, the 2 bright spots were symmetric and possibly mediastinal lymph nodes (Supplemental Fig. 5). On the basis of comparison with non–tumor-bearing mice, the accumulation of the radioactivity in mediastinal nodes was most likely due to tumor metastasis (Supplemental Fig. 5). However, for logistic reasons, no histopathology was performed to confirm the status of these lymph nodes.

DISCUSSION

Imaging plays an important role in the management of patients of metastatic CRC. Anatomic and functional imaging techniques have led to significant improvements in therapeutic interventions and management of metastatic CRC. However, detection of colorectal peritoneal carcinomatosis and pulmonary metastases with imaging remains a challenge, and the performance of different diagnostic methods commonly used is inadequate. In this study, a multimodal approach of T2-weighed MRI with *HER1*-targeted immunoPET was used to successfully detect and image sites of metastases and spread of tumor mass in the peritoneal and thoracic cavities. MRI combined with ^{89}Zr-panitumumab immunoPET revealed *HER1* status and accessibility of mAb to different sites in 3 different models of metastases. Significant differences were observed in the in uptake by *HER1*-positive subcutaneous LS-174T and *HER1*-negative subcutaneous A375 tumors. The cumulative activity in LS-174T tumors was at least 4 times greater than that of A375 tumors (Supplemental Fig. 2). Furthermore, injection of 0.1 mg of panitumumab into the tumor-bearing mice successfully blocked the uptake of ^{89}Zr-labeled panitumumab (Figs. 1B and 3). No differences were observed in the *HER1*-negative A375 model (Fig. 1B; Supplemental

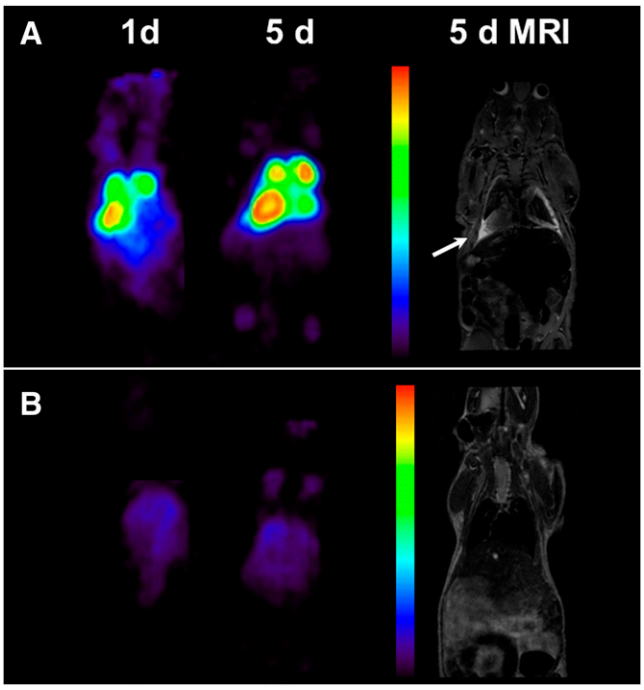

FIGURE 5. Representative reconstructed and processed maximum-intensity PET projections and corresponding T2-weighed coronal MRI slice of female athymic (NCr) *nu/nu* mouse bearing pulmonary metastatic LS-174T tumors (A) and non–tumor-bearing mouse (B). Scale represents percentage of maximum and minimum threshold intensity. Tumors are indicated with arrows.

Fig. 2), therefore demonstrating the *HER1* specificity and targeting of ^{89}Zr-panitumumab.

In addition to changes observed between *HER1*-positive and *HER1*-negative tumor models, ^{89}Zr-panitumumab biodistribution differed in mice bearing LS-174T subcutaneous, intraperitoneal (3- and 7-d tumor burden), and thoracic tumors. Peak tumor uptake of 40 %ID/g was observed at 3–4 d after injection for the subcutaneous model, in contrast to 75 %ID/g at 2 d after injection for the thoracic tumor model and 95 %ID/g at 1–2 d after injection for the intraperitoneal tumor model (Fig. 1; Tables 1 and 2). Tumor uptake in mice bearing 3-d intraperitoneal tumors was almost twice that in mice bearing 7-d intraperitoneal tumors; a positive correlation was observed with tumor uptake and tumor burden (Fig. 2). These observations may be due to multiple factors, including interstitial fluid pressure, tumor vasculature, and target expression in tumors at different locations and sites, which are currently under investigation. Additionally, the role of ascites as a barrier in antibody tumor targeting and disposition also needs to be investigated to better understand the dynamics of using mAbs as targeting vehicles. In addition to tumor uptake, blood clearance was significantly different among the models studied, with the fastest clearance observed in mice bearing intraperitoneal tumors, as compared with the subcutaneous and thoracic tumor models. At 5 d, the levels of radioactivity in the blood of mice bearing intraperitoneal tumors was at least 4.5 times lower than corresponding levels in the blood of mice bearing thoracic tumors (0.78 ± 0.11 vs. 3.70 ± 0.42, respectively). Similarly, the tumor-to-blood ratio for mice bearing intraperitoneal tumors was more than 2.5 times that for mice bearing thoracic tumors at 5 d after injection. The difference in blood clearance may be related to target-mediated drug disposition and may provide some valuable insights into the role of lesion locations and tumor burden on the pharmacokinetics of the radiolabeled antibody. The differential uptake in lesions at different locations has also been observed in patients (*11,16*). In breast cancer patients imaged with ^{89}Zr-trastuzumab, metastatic lesions in the liver had significantly higher uptake than those in the bone and brain (*16*). In squamous cell lung carcinoma patients imaged with ^{111}In-labeled 225 (murine version of cetuximab targeting *HER1*), at least 40 mg of excess 225 coinjection was required to visualize metastatic sites, as compared with 20 mg for primary tumors (*11*). The same study also reported high liver uptake in patients, presumably due to expression of *HER1* in liver hepatocytes, which may pose challenges for imaging of liver metastases. The biodistribution of radiolabeled panitumumab may differ from that of radiolabeled cetuximab because of differences in binding sites and epitope. With successful clinical translation, ^{89}Zr-labeled panitumumab can potentially be used as an imaging tool to provide quantitative information on molecular interactions of panitumumab with *HER1* expressed on primary tumor and metastatic lesions of metastatic CRC. ^{89}Zr-labeled panitumumab can also enable the confirmation of tumor targeting and the quantification of panitumumab accumulation at different target sites and normal organs, particularly when the antibody uptake in the tumor is independent of *HER1* expression measured by immunohistochemistry and Western blot (*14,23*). Imaging with ^{89}Zr-labeled panitumumab may also provide information to determine the target saturation of therapeutic doses at the primary tumor, metastatic lesions, and normal organs. Such information would be beneficial in the design of treatment schedules and adapted to improve treatment efficacy or reduce toxicity and therefore facilitate better management of metastatic CRC patients. However, ^{89}Zr-labeled panitumumab by itself may not predict efficacy or therapeutic outcomes, because other factors such as KRAS and V-raf murine sarcoma viral oncogene homolog B1 (BRAF) mutations are critical for response to panitumumab immunotherapy (*24–26*). Thus, panitumumab imaging may have a complementary role and be best used together with assays to determine v-kis-ras2 Kirsten rat sarcoma viral oncogene mutations and *HER1* gene amplification and polymorphism.

CONCLUSION

As a prelude to clinical translation, a preclinical study with ^{89}Zr-labeled panitumumab was performed. This study demonstrates the potential utility of ^{89}Zr-labeled panitumumab in the assessment of *HER1* status in distant metastases and in understanding the differences in antibody uptake at

different lesion sites. Eventually, ^{89}Zr-labeled panitumumab can play a role in the personalized health care of metastatic CRC to assess target expression and panitumumab accumulation in all tumor lesions and normal tissues, noninvasively and quantitatively.

DISCLOSURE STATEMENT

The costs of publication of this article were defrayed in part by the payment of page charges. Therefore, and solely to indicate this fact, this article is hereby marked "advertisement" in accordance with 18 USC section 1734.

ACKNOWLEDGMENTS

We thank Lawrence Szajek (Clinical Center, NIH) for his assistance in irradiating the yttrium target. This research was supported by the Intramural Research Program of the National Institutes of Health, National Cancer Institute, and Center for Cancer Research, and the U.S. Department of Health and Human Services. No other potential conflict of interest relevant to this article was reported.

REFERENCES

1. Jemal A, Bray F, Center MM, Ferlay J, Ward E, Forman D. Global cancer statistics. *CA Cancer J Clin.* 2011;61:69–90.
2. Maggiori L, Elias D. Curative treatment of colorectal peritoneal carcinomatosis: current status and future trends. *Eur J Surg Oncol.* 2010;36:599–603.
3. Mitry E, Guiu B, Cosconea S, Jooste V, Faivre J, Bouvier AM. Epidemiology, management and prognosis of colorectal cancer with lung metastases: a 30-year population-based study. *Gut.* 2010;59:1383–1388.
4. Normanno N, De Luca A, Salomon DS, Ciardiello F. Epidermal growth factor-related peptides as targets for experimental therapy of human colon carcinoma. *Cancer Detect Prev.* 1998;22:62–67.
5. Ciardiello F, Kim N, Saeki T, et al. Differential expression of epidermal growth factor-related proteins in human colorectal tumors. *Proc Natl Acad Sci USA.* 1991;88:7792–7796.
6. Mayer A, Takimoto M, Fritz E, Schellander G, Kofler K, Ludwig H. The prognostic significance of proliferating cell nuclear antigen, epidermal growth factor receptor, and mdr gene expression in colorectal cancer. *Cancer.* 1993;71:2454–2460.
7. Amador ML, Hidalgo M. Epidermal growth factor receptor as a therapeutic target for the treatment of colorectal cancer. *Clin Colorectal Cancer.* 2004;4:51–62.
8. Chung KY, Shia J, Kemeny NE, et al. Cetuximab shows activity in colorectal cancer patients with tumors that do not express the epidermal growth factor receptor by immunohistochemistry. *J Clin Oncol.* 2005;23:1803–1810.
9. Hebbar M, Wacrenier A, Desauw C, et al. Lack of usefulness of epidermal growth factor receptor expression determination for cetuximab therapy in patients with colorectal cancer. *Anticancer Drugs.* 2006;17:855–857.
10. van Dongen GA, Vosjan MJ. Immuno-positron emission tomography: shedding light on clinical antibody therapy. *Cancer Biother Radiopharm.* 2010;25:375–385.
11. Divgi CR, Welt S, Kris M, et al. Phase I and imaging trial of indium 111-labeled anti-epidermal growth factor receptor monoclonal antibody 225 in patients with squamous cell lung carcinoma. *J Natl Cancer Inst.* 1991;83:97–104.
12. Nayak TK, Brechbiel MW. Radioimmunoimaging with longer-lived positron-emitting radionuclides: potentials and challenges. *Bioconjug Chem.* 2009;20:825–841.
13. Niu G, Li Z, Xie J, Le QT, Chen X. PET of EGFR antibody distribution in head and neck squamous cell carcinoma models. *J Nucl Med.* 2009;50:1116–1123.
14. Nayak TK, Garmestani K, Baidoo KE, Milenic DE, Brechbiel MW. Preparation, biological evaluation, and pharmacokinetics of the human anti-HER1 monoclonal antibody panitumumab labeled with 86Y for quantitative PET of carcinoma. *J Nucl Med.* 2010;51:942–950.
15. Nayak TK, Garmestani K, Milenic DE, Baidoo KE, Brechbiel MW. HER1-targeted ^{86}Y-panitumumab possesses superior targeting characteristics than ^{86}Y-cetuximab for PET imaging of human malignant mesothelioma tumors xenografts. *PLoS ONE.* 2011;6:e18198.
16. Dijkers EC, Oude Munnink TH, Kosterink JG, et al. Biodistribution of ^{89}Zr-trastuzumab and PET imaging of HER2-positive lesions in patients with metastatic breast cancer. *Clin Pharmacol Ther.* 2010;87:586–592.
17. Dadachova E, Chappell LL, Brechbiel MW. Spectrophotometric method for determination of bifunctional macrocyclic ligands in macrocyclic ligand-protein conjugates. *Nucl Med Biol.* 1999;26:977–982.
18. Meares CF, McCall MJ, Reardan DT, Goodwin DA, Diamanti CI, McTigue M. Conjugation of antibodies with bifunctional chelating agents: isothiocyanate and bromoacetamide reagents, methods of analysis, and subsequent addition of metal ions. *Anal Biochem.* 1984;142:68–78.
19. Ray GL, Baidoo KE, Wong KJ, et al. Preclinical evaluation of a monoclonal antibody targeting the epidermal growth factor receptor as a radioimmunodiagnostic and radioimmunotherapeutic agent. *Br J Pharmacol.* 2009;157:1541–1548.
20. Nayak TK, Regino CA, Wong KJ, et al. PET imaging of HER1-expressing xenografts in mice with 86Y-CHX-A″-DTPA-cetuximab. *Eur J Nucl Med Mol Imaging.* 2010;37:1368–1376.
21. Milenic DE, Garmestani K, Brady ED, et al. Multimodality therapy: potentiation of high linear energy transfer radiation with paclitaxel for the treatment of disseminated peritoneal disease. *Clin Cancer Res.* 2008;14:5108–5115.
22. Gibaldi M, Perrier D. *Pharmacokinetics*. 2nd ed. New York, NY: Dekker; 1982.
23. Aerts HJ, Dubois L, Perk L, et al. Disparity between in vivo EGFR expression and ^{89}Zr-labeled cetuximab uptake assessed with PET. *J Nucl Med.* 2009;50:123–131.
24. Peeters M, Siena S, Van Cutsem E, et al. Association of progression-free survival, overall survival, and patient-reported outcomes by skin toxicity and KRAS status in patients receiving panitumumab monotherapy. *Cancer.* 2009;115:1544–1554.
25. Amado RG, Wolf M, Peeters M, et al. Wild-type KRAS is required for panitumumab efficacy in patients with metastatic colorectal cancer. *J Clin Oncol.* 2008;26:1626–1634.
26. Bardelli A, Siena S. Molecular mechanisms of resistance to cetuximab and panitumumab in colorectal cancer. *J Clin Oncol.* 2010;28:1254–1261.